


One-component plasma of a million particles via angular-averaged Ewald potential: A Monte Carlo study

G. S. Demyanov * and P. R. Levashov 

Joint Institute for High Temperatures, Izhorskaya 13 Bldg 2, Moscow 125412, Russia
and Moscow Institute of Physics and Technology, Institutskiy Pereulok 9, Dolgoprudny, Moscow Region, 141701, Russia

 (Received 3 May 2022; accepted 30 June 2022; published 26 July 2022)

In this work we derive a correct expression for the one-component plasma (OCP) energy via the angular-averaged Ewald potential (AAEP). Unlike Yakub and Ronchi [J. Low Temp. Phys. **139**, 633 (2005)], who had tried to obtain the same energy expression from a two-component plasma model, we used the original Ewald potential for an OCP. A constant in the AAEP was determined using the cluster expansion in the limit of weak coupling. The potential has a simple form suitable for effective numerical simulations. To demonstrate the advantages of the AAEP, we performed a number of Monte Carlo simulations for an OCP with up to a million particles in a wide range of the coupling parameter. Our computations turned out at least two orders of magnitude more effective than those with a traditional Ewald potential. A unified approach is offered for the determination of the thermodynamic limit in the whole investigated range. Our results are in good agreement with both theoretical data for a weakly coupled OCP and previous numerical simulations. We hope that the AAEP will be useful in path integral Monte Carlo simulations of the uniform electron gas.

DOI: [10.1103/PhysRevE.106.015204](https://doi.org/10.1103/PhysRevE.106.015204)

I. INTRODUCTION

A one-component plasma (OCP) is an important and well-studied model with a long history [1–7]. An OCP is usually defined as a system of point ions immersed in a uniform neutralizing background [8]. An OCP is a good approximation of a two-component plasma (TCP) if the ions can be considered classical (their de Broglie wavelength is much less than the interionic distance) and the electrons are highly degenerated. Such conditions correspond to the interior of Jupiter (for hydrogen ions), white dwarfs (for helium, carbon, and oxygen ions), and neutron star crusts (e.g., for iron ions) and can also be obtained in laser experiments [3]. A quantum-mechanical analog of the OCP is the well-known “jellium” model introduced by Wigner in 1938 [9] that has received much attention in the last decade [10–13].

Contrary to a classical TCP, an OCP satisfies the so-called H -stability condition classically; the thermodynamic limit exists for its thermodynamic properties in both the micro-canonical and canonical ensembles [14]. Another advantage of the OCP is the dependence of all its properties only on a dimensionless coupling parameter Γ [1, Sec. II], [15, §31, Problem 1], [8].

On the other hand, the long-range Coulomb interaction between the ions should be taken into account. This causes significant difficulties in both analytical and numerical studies. In particular, the electrostatic energy of an infinite OCP is a conditionally convergent series, so the summation result depends on the order of the terms [16]. For crystalline Coulomb systems, the solution to this problem was proposed

by Ewald [17]. Adding to and subtracting from the original sum a system of normally distributed screening charges, one may transform the sum into two rapidly converging series. This procedure defines an anisotropic short-ranged Ewald potential [1,3,8], which is used in further analysis.

In computer simulations, a cubic box with periodic boundary conditions is often used, so a system without a long-range order acquires a translational symmetry. The Ewald’s summation technique is also valid in this case; therefore, almost all Monte Carlo (MC) or molecular dynamics (MD) studies of an OCP are based upon this approach.

Many different approaches have been developed to implement the Ewald’s technique in computations. The traditional Ewald summation (5) requires the computational cost of the order $O(N^2)$. The grid-based Ewald methods, such as particle-mesh Ewald [18], smoothed particle-mesh Ewald [19], and particle-particle-particle mesh [20, Chapter 8], allow one to reduce the complexity to $O(N \log N)$. In our work and most of the ones cited below, the traditional Ewald approach is used.

In 1966 the first extensive numerical investigation of an OCP was carried out by Brush, Sahlin, and Teller using a MC method [8]. The authors calculated thermodynamic properties and radial distribution functions (RDFs) in the range $0.05 \leq \Gamma \leq 100$, which corresponds to the fluid state. However, a small number of particles $N \leq 500$ was used, being especially critical at $\Gamma \ll 1$ when the Debye length becomes large [7]; the thermodynamic limit was not considered.

In 1973 the well-known work by Hansen [1] was published, in which the equation of state of a fluid OCP was constructed using MC simulation data in the range $1 \leq \Gamma \leq 160$. The number of particles in the cell was also small, $N \leq 250$; the thermodynamic limit was not investigated. The anisotropic part of the Ewald potential was approximated by an optimized

*Corresponding author: demyanov.gs@phystech.edu

expansion in Kubic harmonics; its accuracy was criticized in Ref. [2, Sec. II]. Also, a detailed examination shows that there are some misprints in the formulas in Ref. [1, e.g., Eq. (7) or (B3)].

In Ref. [2], Slattery, Doolen, and DeWitt used a more precise approximation for the Ewald potential compared to [1,8]. The authors examine both the fluid and solid phases of an OCP ($1 \leq \Gamma \leq 300$). Using $N = 128$, they built the equation of state for both phases and estimated the fluid-solid transition point as $\Gamma_m = 168 \pm 4$. The N dependence was considered by the same authors only in the following paper [21]. In Ref. [21] a linear dependence on N^{-1} is assumed. The thermodynamic limit was found by the extrapolation of MC data. Nevertheless, the authors state that they do not know the correct dependence on N , although the proposed dependence fits the MC data well. In Ref. [21] the authors present a significantly different value of $\Gamma_m = 178 \pm 1$.

As we see, the convergence of the results on N is the major question of all such studies, including the calculation of Γ_m . This important aspect is discussed in [22], where $N \leq 1024$ was used. The “center-of-mass correction” of the OCP energy is considered. This correction was applied, e.g., in [1, Eq. (16)], [21]. The authors conclude that this correction cannot be justified for the fluid OCP but is necessary for the solid phase.

Significant progress in the accuracy of MC simulation results was made in the works by Caillol *et al.* [7,23–27]. Starting from [23], they developed a method for modeling an OCP on the sphere surface of different dimensions. They demonstrated in detail the ability of this approach by simulating a 2D OCP [24] using $N \leq 256$ in the $0.5 \leq \Gamma \leq 200$ region. In [25] Caillol discusses the difference between simulations in a cubic cell and on a sphere surface from a theoretical point of view.

Using this method, the most reliable result for the OCP energy was obtained in [26] for $1 \leq \Gamma \leq 190$ and in [7] for $0.1 \leq \Gamma \leq 1$. The authors consider the thermodynamic limit in both papers; $N \leq 3200$ is used in [26] and $N \leq 51200$ in [7]. To reduce the statistical error, a record number of configurations (10^8 – 10^9) were used in MC simulations.

It can be seen from the above that over time, more and more attention has been paid to the problem of the N dependence in OCP MC simulations. Modern computers made it possible to increase the number of particles in OCP MC simulations from $N = 10^2$ in 1966 [8] to $N = 5 \times 10^4$ in 2010 [7], respectively, as well as significantly decrease the statistical error. We also see that the statement in [3, bottom of p. 19] about a weak dependence of the OCP energy on N is simply wrong.

As for the MD, it is mainly applied to investigate the dynamic and transport properties of an OCP [27–29], including in the presence of external fields [30–32]. The first reference to such a simulation was given in [8], and the first “extensive” study was done by Hansen *et al.* [33,34]. In these works, the authors present the computations of the velocity autocorrelation function and the dynamical structure factor. The thermal conductivity and viscosity of an OCP are calculated in [35] using the Kubo formula. The OCP internal energy can also be obtained from MD simulations [36], as well as the estimations of the fluid-solid transition point Γ_m [37].

Using MD simulations one may investigate the OCP system with the Yukawa potential (YOCP) [38,39], including the low screening limit [40]. In such a regime the YOCP results tend to the OCP ones [41].

Two main theoretical approaches for an OCP have been developing: the theory of integral equations for an RDF, $g(r)$, and the expansion of the internal energy on Γ . Starting from the Debye and Hückel [42] result, in which the expansion of the internal energy up to the term $\Gamma^{3/2}$ was obtained, there has been significant progress. In Ref. [43] the diagram technique was used for this purpose. According to Caillol [7], further development by Ortner [44] produced no significant difference from the result of [43]. Nevertheless, these studies have made the expansion applicable at $\Gamma \leq 0.3$, whereas the result by Debye and Hückel is reliable only at $\Gamma \leq 0.01$. The work by Brilliantov [45] derives the approximate “first-principle” OCP equation of state, demonstrating the error of 2%–5% in the range $0 \leq \Gamma \leq 250$.

Nevertheless, the expansion on Γ does not produce relatively accurate results even at $\Gamma = 1$ [7, Fig. 1], [3, p. 27]. At higher Γ , the theory of integral equations for an RDF was applied. In particular, the hypernetted chain (HNC) approximation [46] gives quite accurate results for the energy at $\Gamma \leq 1$, as was shown in [7, Fig. 1] and [3, Sec. 3.7]. As well as for an OCP, this theory can be implemented for a YOCP, using the Rogers-Young, Ballone-Pastore-Galli-Gazzillo, and variational modified HNC [47] and the soft mean spherical [48] approximations. However, at stronger interaction, integral equations should be corrected to agree with MC or MD results [49–51].

Thus, despite the development of various theoretical methods, numerical modeling is indispensable in the study of an OCP. As a consequence, there is a request for fast and efficient calculation methods that can produce highly accurate results. To reduce the amount of computations in the usual Ewald technique, Yakub and Ronchi [52] proposed an angular-averaged Ewald potential (AAEP) for the simulation of an isotropic Coulomb TCP. Indeed, as the Ewald potential is anisotropic, it seems redundant to apply it to isotropic plasma systems. The AAEP was correctly presented for a TCP without a clear derivation [52]. It was successfully used in computations [53–64], including the simulation of quantum systems [11–13]. Recently we have succeeded in finding a step-by-step derivation of the AAEP for a TCP [65]. Yakub and Ronchi computed the OCP energy from the TCP one; the AAEP in the case of an OCP was not presented. However, the energy expression given in [66, Eq. (8)], [53, Eq. (8)] is wrong and has no step-by-step derivation either. This confusion stimulated us to derive a correct expression for the OCP AAEP by the direct averaging of the Ewald potential (6). This paper is devoted to solving this problem. Also we obtain the correct expression for the OCP energy. Finally, we perform MC simulations for a fluid OCP using up to a *million* particles to obtain precise values of energy.

The paper is organized as follows. Section II contains the problem statement and the derivation of the AAEP for the case of the OCP. In Sec. III we make the correction of the AAEP and obtain the correct expression for the OCP energy. Section IV is devoted to the applications of the new potential including MC simulations of the OCP energy with up to a

million particles in a wide range of the coupling parameter. We discuss our computational results in Sec. V. The conclusion is formulated in Sec. VI.

II. AVERAGING THE OCP EWALD POTENTIAL

In this section, we derive an expression for the AAEP in an OCP, examine its main properties and make it suitable for numerical calculations.

A. Problem statement

Consider a cubic cell with a side length L . This cell contains N positively charged particles at positions \mathbf{r}_i , $i = 1, \dots, N$. All the particles have equal charge $Ze > 0$, $e > 0$, and Z is a charge number. Negative charge with density $-NZe/L^3$ uniformly distributed throughout the cell ensures electroneutrality. We call this cell the main cell. The cell repeats itself in the three mutually perpendicular directions; each i th particle has an infinite number of images with positions $\mathbf{r}_i + \mathbf{n}L$. Here \mathbf{n} is an integer vector $\mathbf{n} = (n_x, n_y, n_z)$, $n_x, n_y, n_z \in \mathbb{Z}$. Then the negatively charged uniform background occupies the entire space with the same charge density. We call such an infinite electroneutral system the OCP. Now at some point $\mathbf{r} \in \mathbb{R}^3$, we have the following charge density $w(\mathbf{r})$:

$$w(\mathbf{r}) = Ze \sum_{i=1}^N \sum_{\mathbf{n}} \delta(\mathbf{r} - \mathbf{r}_i - \mathbf{n}L) - N \frac{Ze}{L^3}. \quad (1)$$

Here $\delta(\mathbf{r} - \mathbf{r}_i)$ is the Dirac δ function, and $\sum_{\mathbf{n}}$ denotes a summation over all integer vectors \mathbf{n} . An interaction potential between positively charged particles $\phi(\mathbf{r})$ satisfies the Poisson equation (in Gaussian units):

$$\Delta \phi(\mathbf{r}) = -4\pi w(\mathbf{r}), \quad (2)$$

where Δ is the Laplacian.

The excess thermodynamic properties of the OCP depend only on the dimensionless parameter Γ [1, Sec. II], [15, §31, Problem 1]:

$$\Gamma = \frac{(Ze)^2}{k_B T a}, \quad (3)$$

where $a^3 \equiv \frac{3}{4\pi\rho}$ is the ‘‘ion-sphere radius,’’ $\rho = N/L^3$ is the number density, T is the temperature of the system, and k_B is the Boltzmann constant. The value of Γ denotes the ratio of a characteristic potential energy to a characteristic kinetic energy of particles. The $\Gamma \ll 1$ regime corresponds to a weakly coupled OCP in which the kinetic energy dominates over the potential one. From the definitions of a and ρ , there is a useful relationship between L and N :

$$(L/a)^3 = 4\pi N/3. \quad (4)$$

We use a as the unit of length in all subsequent formulas.

The energy of the OCP can be written in terms of the effective interaction potential between particles in the main cell. This pair potential $v(\mathbf{r})$ is given in [1, Eq. (5)], [8, Eqs. (11)–(13)]; it takes into account the presence of the

negatively charged background. Then the ratio of the OCP total potential energy E^{Ew} to $k_B T$, $U \equiv E/(k_B T)$, reads

$$U^{\text{Ew}}(\Gamma) = U_0(\Gamma) + \frac{\Gamma}{2} \sum_{i=1}^N \sum_{\substack{j=1 \\ j \neq i}}^N v(\mathbf{r}_{ij}), \quad (5)$$

$$v(\mathbf{r}) = v_1(r) + v_2(\mathbf{r}), \quad (6)$$

$$Lv_1(r) = \frac{\text{erfc}(\sqrt{\pi}r/L)}{r/L} - 1, \quad (7)$$

$$Lv_2(\mathbf{r}) = \sum_{\mathbf{n} \neq \mathbf{0}} \left[\frac{\text{erfc}(\sqrt{\pi}|\mathbf{r}/L + \mathbf{n}|)}{|\mathbf{r}/L + \mathbf{n}|} + \frac{e^{-\pi n^2}}{\pi n^2} \cos\left(\frac{2\pi}{L} \mathbf{r} \cdot \mathbf{n}\right) \right], \quad (8)$$

where $\mathbf{r}_{ij} = \mathbf{r}_i - \mathbf{r}_j$, $n = |\mathbf{n}| = (n_x^2 + n_y^2 + n_z^2)^{1/2}$, $r = |\mathbf{r}|$. The potential $v(\mathbf{r})$ is called the Ewald potential. Summation $\sum_{\mathbf{n} \neq \mathbf{0}}$ means that the term $\mathbf{n} = (0, 0, 0) \equiv \mathbf{0}$ is omitted. The potential $v(\mathbf{r})$ consists of a spherically symmetrical $v_1(r)$ and angular dependent $v_2(\mathbf{r})$ parts. Since the right-hand sides of Eqs. (7) and (8) are dependent on the ratio \mathbf{r}/L we introduce the notation:

$$\mathbf{x} \equiv \mathbf{r}/L, \quad x \equiv r/L. \quad (9)$$

The energy expression (5) contains the summation over N particles only. The interaction between all the periodic particle images is included in the Ewald potential (8). Thus, a particle in the main cell interacts only with $N - 1$ other particles in the main cell or with the nearest ‘‘images’’ in one of the neighboring cells. Such a procedure corresponds to the ‘‘minimum-image convention.’’ As a result, for fixed particle positions, each particle interacts with $N - 1$ particles that are located in a cube centered at that particle [8, Sec. III], [65, Sec. IV].

The first term U_0 in (5) denotes the self-interaction energy between particles with their replicas. This term depends on the potential $v(\mathbf{r})$ [8, Eq. (10)]:

$$U_0(\Gamma) = \frac{\Gamma}{2} N \lim_{|\mathbf{r}| \rightarrow 0} \left(v(\mathbf{r}) - \frac{1}{r} \right) = -\frac{1}{2} N^{2/3} \Gamma M_{sc}. \quad (10)$$

Here $M_{sc} = 1.760118884$ is the Madelung constant of a simple cubic lattice. The last equality in Eq. (10) is valid only for the Ewald potential (6). Note that the formula for the self-interacting term given in [1, see Eq. (7)] is false.

B. Averaging the Ewald potential

In disordered media, the angular dependence of $v_2(\mathbf{r})$ leads to needless calculations since all orientations are equivalent. First, we directly apply the approach of Yakub and Ronchi, which was used earlier for a TCP [52,65], to average $v_2(\mathbf{r}_{ij})$ over all directions at a distance r_{ij} :

$$v_2^a(r_{ij}) = \frac{1}{4\pi} \int_{-1}^1 d(\cos \theta) \int_0^{2\pi} v_2(\mathbf{r}_{ij}) d\psi. \quad (11)$$

The module in the first term of $v_2(\mathbf{r})$ in Eq. (8) has the following form ($\mathbf{n} \cdot \mathbf{x} = nx \cos \theta$):

$$|\mathbf{x} + \mathbf{n}| = \sqrt{x^2 + n^2 + 2nx \cos \theta}. \quad (12)$$

Now we can integrate it over angles:

$$\frac{1}{2} \int_{-1}^1 d(\cos \theta) \frac{\operatorname{erfc}(\sqrt{\pi}|\mathbf{x} + \mathbf{n}|)}{|\mathbf{x} + \mathbf{n}|} = \frac{f(|n-x|) - f(|n+x|)}{2\pi nx}, \quad (13)$$

where

$$f(n) = e^{-\pi n^2} - \pi n \operatorname{erfc}(\sqrt{\pi}n). \quad (14)$$

Averaging the second term in Eq. (8)

$$\frac{1}{2} \int_{-1}^1 d(\cos \theta) \cos(2\pi xn \cos \theta) = \frac{\sin(2\pi xn)}{2\pi xn}, \quad (15)$$

we obtain the angular-averaged pair potential $v_2^a(x)$:

$$Lv_2^a(x) = \frac{1}{2\pi nx} \sum_{n \neq 0} \left[f(|n-x|) - f(|n+x|) + \frac{e^{-\pi n^2}}{\pi n^2} \sin(2\pi nx) \right]. \quad (16)$$

Further we are going to consider only the case of $x < 1$ (see the explanation below and [65, Sec. IV]). Since the minimum value of n is 1, we will reveal the module as follows: $|n-x| = n-x$. Next, we expand $v^a(x) = v_1(x) + v_2^a(x)$ into the converging series by x at $x = 0$:

$$\begin{aligned} Lv^a(x) &= \frac{\operatorname{erfc}(\sqrt{\pi}x)}{x} - 1 + Lv_2^a(x) \\ &= \frac{1}{x} - C_0 + \frac{2\pi x^2}{3} + \sum_{k=2}^{\infty} C_k x^{2k}. \end{aligned} \quad (17)$$

The coefficient C_0 is related to the Madelung constant of a simple cubic lattice, M_{sc} :

$$\begin{aligned} C_0 &= 3 - \sum_{n \neq 0} \left(\frac{\operatorname{erfc}(\sqrt{\pi}n)}{n} + \frac{e^{-\pi n^2}}{\pi n^2} \right) \\ &= - \lim_{x \rightarrow 0} \left(Lv(\mathbf{x}) - \frac{1}{x} \right) = M_{sc} (4\pi/3)^{1/3}. \end{aligned} \quad (18)$$

The general formula for the series coefficients (for $k \geq 1$) is derived in Appendix A and given in Eq. (A14). We rigorously prove in Appendix B that $C_k = 0$ for $k \geq 2$. Thus, the expression for the OCP AAEP is

$$v^a(r) = \frac{1}{r} \left[1 - M_{sc} \frac{r}{r_m} + \frac{1}{2} \left(\frac{r}{r_m} \right)^3 \right], \quad (19)$$

where

$$r_m = \left(\frac{3}{4\pi} \right)^{1/3} L = N^{1/3} < L \quad (20)$$

is the radius of the sphere $4\pi r_m^3/3 = L^3$ with equivalent volume L^3 . The last relation is obtained using Eq. (4). Note that $L/2 < r_m$. The expression for the AAEP in case of an OCP was not presented in the original works [53,66].

The AAEP reaches its minimum value $v^a(r_m) = [3/2 - M_{sc}]/r_m$ at $r = r_m$, $\partial v^a(r)/\partial r|_{r=r_m} = 0$. For $L > r > r_m$, the potential increase; this behavior is incorrect (see [65, Sec. IV]). Thus, one must consider Eq. (19) up to a point

$r = r_m$; we redefine $v^a(r)$ by zero for $r > r_m$:

$$v^a(r > r_m) = 0. \quad (21)$$

Each particle is affected by $N_s - 1$ particles in the sphere of a radius r_m . Here N_s is the full number of particles in the sphere with a center at some ion; this number is dependent on the position (more details are given in our previous paper [65, Secs. IV, V]). Below we show that the average value of \bar{N}_s during the MC simulation matches the value N (see Fig. 3).

The term $-M_{sc}r/r_m$ in Eq. (19) is responsible for the background negative charge. Our calculations show that the coefficient M_{sc} leads to the divergence of the potential energy per ion as the number N increases. The reason for such behavior is assumed to be related to the angular averaging. Therefore, the coefficient M_{sc} must be changed. Below we obtain the correct value for the coefficient from the cluster expansion.

III. CORRECTION AND SHIFTING OF THE POTENTIAL

In this section, we correct the constant coefficient in the AAEP and obtain the final OCP energy expression (38), which can be used in applications.

A. Correction of the AAEP

Now we consider the AAEP (19) with an unknown coefficient: $M_{sc} \rightarrow C$. The excess part of the canonical partition function for a system of N particles interacting through potential (19) is [1, Sec. III]

$$\begin{aligned} Q_N(\Gamma) &= \int \cdots \int \exp \left[-\Gamma \sum_{i < j} v^a(r_{ij}) \right] d^3 r_1 \cdots d^3 r_N \\ &= \int \cdots \int \prod_{i < j} \exp[-\Gamma v^a(r_{ij})] d^3 r_1 \cdots d^3 r_N. \end{aligned} \quad (22)$$

Here the integration region over each coordinate is a volume $L^3 = 4\pi N/3$. We define the Mayer f function,

$$\exp[-\Gamma v^a(r_{ij})] = 1 + f_{ij}, \quad (23)$$

and rewrite the partition function:

$$Q_N(\Gamma) = \int \cdots \int \prod_{i < j} (1 + f_{ij}) d^3 r_1 \cdots d^3 r_N. \quad (24)$$

Providing the cluster expansion

$$\prod_{i < j} (1 + f_{ij}) = 1 + \sum_{i < j} f_{ij} + \cdots, \quad (25)$$

we get in the first order of f_{ij}

$$\begin{aligned} Q_N(\Gamma) &\approx \int \cdots \int \left(1 + \sum_{i < j} f_{ij} \right) d^3 r_1 \cdots d^3 r_N \\ &= \left(\frac{4\pi}{3} N \right)^N + \sum_{i < j} \int \cdots \int f_{ij} d^3 r_1 \cdots d^3 r_N. \end{aligned} \quad (26)$$

After the integration, the last term has the form

$$\begin{aligned} & \sum_{i < j} \int \cdots \int f_{ij} d^3 r_1 \cdots d^3 r_N \\ &= -\frac{N(N-1)}{2} \left(\frac{4\pi}{3} N\right)^N \\ & \quad + \frac{N(N-1)}{2} \left(\frac{4\pi}{3} N\right)^{N-2} I(\Gamma, N), \end{aligned} \quad (27)$$

where $I(\Gamma, N)$ is the following integral:

$$\begin{aligned} I(\Gamma, N) &= \int d\mathbf{r}_i \int \exp[-\Gamma v^a(|\mathbf{r}_j - \mathbf{r}_i|)] d(\mathbf{r}_j - \mathbf{r}_i) \\ &= \int d\mathbf{r}_i \int_0^{r_m} \exp[-\Gamma v^a(u)] 4\pi u^2 du \\ &= 3 \left(\frac{4\pi}{3} N\right)^2 K(\Gamma, N), \end{aligned} \quad (28)$$

$$K(\Gamma, N) = \int_0^1 \exp[-\Gamma v^a(sr_m)] s^2 ds, \quad (29)$$

$$v^a(sr_m) = \frac{1}{r_m} \left(\frac{1}{s} - C + \frac{s^2}{2} \right). \quad (30)$$

Thus, we get the final expression for the excess part of the canonical partition function in the first order of the cluster expansion:

$$Q_N(\Gamma) \approx \left(\frac{4\pi}{3} N\right)^N \left\{ 1 + \frac{N(N-1)}{2} [3K(\Gamma, N) - 1] \right\}. \quad (31)$$

The potential energy E_{cl} then reads

$$\begin{aligned} \frac{E_{cl}}{Nk_B T}(\Gamma) &= -\frac{1}{\Gamma} \frac{1}{Q_N(\Gamma)} \frac{\partial Q_N(\Gamma)}{\partial \Gamma} \\ &\approx -\frac{1}{\Gamma} \frac{1}{\frac{2/3}{N(N-1)} + K(\Gamma, N) - 1/3} \frac{\partial K(\Gamma, N)}{\partial \Gamma}. \end{aligned} \quad (32)$$

With $\Gamma \rightarrow 0$, the derivative

$$\begin{aligned} \frac{\partial K(\Gamma, N)}{\partial \Gamma} &= -\frac{1}{r_m} \int_0^1 \left(\frac{1}{s} - C + \frac{s^2}{2} \right) \\ & \quad \times \exp \left[2 \ln s - \frac{\Gamma}{r_m} \left(\frac{1}{s} - C + \frac{s^2}{2} \right) \right] ds \end{aligned} \quad (33)$$

must tend to zero since $\Gamma \rightarrow 0$ corresponds to the ideal gas and $E_{cl}/(Nk_B T)(0) = 0$ for any N . From this condition, we find the unknown value of C :

$$\frac{\partial K(\Gamma \rightarrow 0, N)}{\partial \Gamma} = 0 \Rightarrow C = 9/5. \quad (34)$$

The final expression for the AAEP (19) should be used with $M_{sc} \rightarrow C = 9/5$. The self-interaction energy U_0 also should

be changed to U_{0a} in accordance with (10):

$$U_{0a}(\Gamma) = \frac{\Gamma}{2} N \lim_{r \rightarrow 0} \left(v^a(r) - \frac{1}{r} \right) = -\frac{1}{2} N^{2/3} \Gamma C. \quad (35)$$

B. Shifting the potential

Discontinuity of $v^a(r)$ at the point $r = r_m$ results in a discontinuity in the energy. Such behavior leads to different problems during numerical simulations [67, p. 302]. Thus, it is reasonable to shift the average potential to make it zero at $r \geq r_m$. The contribution of the two-particle interaction to the internal energy is the following:

$$\begin{aligned} & \frac{\Gamma}{2} \sum_{i=1}^N \sum_{\substack{j=1 \\ j \neq i}}^N [v^a(r_{ij}) - v^a(r_m) + v^a(r_m)] \\ &= \frac{N(N-1)\Gamma}{2} v^a(r_m) + \frac{\Gamma}{2} \sum_{i=1}^N \sum_{\substack{j=1 \\ j \neq i}}^N \tilde{v}(r_{ij}), \end{aligned} \quad (36)$$

where the pair potential $\tilde{v}(r)|_{r \leq r_m} = v^a(r)|_{r \leq r_m} - v^a(r_m)$ has the form

$$\tilde{v}(r) = \begin{cases} \frac{1}{r} \left\{ 1 + \frac{1}{2} \left(\frac{r}{r_m} \right) \left[\left(\frac{r}{r_m} \right)^2 - 3 \right] \right\}, & r < r_m \\ 0, & r \geq r_m \end{cases}. \quad (37)$$

Since the number of ions in the sphere differs from N , we replace $\sum_{\substack{j=1 \\ j \neq i}}^N \tilde{v}(r_{ij})$ with $\sum_{\substack{j=1 \\ j \neq i}}^{N_{s,i}} \tilde{v}(r_{ij})$ in (36). Here $N_{s,i}$ is the number of ions in the sphere centered at an i th ion. The full potential energy then reads

$$U(\Gamma) = \tilde{U}_0(\Gamma) + \frac{\Gamma}{2} \sum_{i=1}^N \sum_{\substack{j=1 \\ j \neq i}}^{N_{s,i}} \tilde{v}(r_{ij}). \quad (38)$$

The constant term in (38)

$$\begin{aligned} \tilde{U}_0(\Gamma) &= U_{0a}(\Gamma) + \frac{N(N-1)\Gamma}{2} v^a(r_m) \\ &= -\frac{N^{2/3}\Gamma C}{2} + \frac{N(N-1)}{2r_m} \left(\frac{3}{2} - C \right) \Gamma \\ &= -\frac{3}{20} N^{2/3} \Gamma (N+5) \end{aligned} \quad (39)$$

includes both the effects of self-interaction and shifting of AAEP. Here we used $C = 9/5$ (34) and $r_m = N^{1/3}$ (20).

So, to calculate the OCP energy, one needs to evaluate the interaction of any ion placed in the center of a sphere with a radius r_m with all other ions inside this sphere and then sum up all such interactions. Each i th particle interacts only with $N_{s,i} - 1$ particles that are located in a sphere centered at the i th particle.

One may notice that the radius of interaction $r_m > L/2$; thus, the influence of some ions should be taken twice. This was explained in more detail in [52, Sec. III], [54, Sec. 2], and [65, Sec. V].

The potential (37) can also be applied in MD simulations. Since $\tilde{v}(r)$ is a smooth function, we calculate a force $\mathbf{f}(r)$

between two particles as follows:

$$\mathbf{f}(\mathbf{r}) = -\frac{(Ze)^2}{a^2} \nabla \tilde{v}(r) = \frac{(Ze)^2}{a^2} \mathbf{r} \times \begin{cases} \frac{1}{r^3} - \frac{1}{r_m^3}, & r < r_m, \\ 0, & r \geq r_m \end{cases}, \quad (40)$$

where ∇ is the gradient operator.

In Ref. [66, Eq. (8)], the formula for the OCP potential energy is given without derivation. For clarity, we reproduce the wrong formula [66, Eq. (8)] here (in the Gaussian units):

$$U_N^{(\text{OCP})} = -0.9 \frac{NQ^2}{r_m} + \frac{1}{2} \sum_{i=1}^N \sum_{\substack{j=1 \\ j \neq i}}^N Q^2 \tilde{v}(r_{ij}). \quad (41)$$

It has the same form as Eq. (38), but the constant term $\tilde{U}_0(\Gamma)$ is incorrect. Nevertheless, Yakub and Ronchi published correct results for the Madelung constants and the OCP energy. The correct formula (38) with a rigorous derivation from the Ewald potential is the main result of this paper.

In Ref. [65] we derive the TCP energy expressed through the averaged TCP Ewald potential. Replacing in this formula the summation over negatively charged particles with the integration over a uniformly distributed background, it is possible to obtain the OCP energy (38). We provide such a derivation in Appendix C.

IV. APPLICATIONS

Below we demonstrate accurate calculations for the OCP with the AAEP. We calculate the Madelung constants for two lattices, examine the performance of the calculation algorithm, and present the results of MC simulations with *one million* particles.

A. Madelung constant

In this subsection, we use the AAEP (19) to calculate the Madelung constant M of body-centered cubic (bcc) and face-centered cubic (fcc) lattices to verify our procedure of energy calculation. The expression for M in case of (38) takes the following form:

$$M = -\frac{3}{20} N^{-1/3} (N + 5) + \frac{1}{2} \sum_{\substack{j=1 \\ j \neq i}}^{N_s} \tilde{v}(r_{ij}). \quad (42)$$

The results can be seen in Tables I and II for bcc and fcc lattices, respectively. Even though the number of ions in the sphere N_s differs from N and the ionic configuration is not spherically symmetric at all, we observe the convergence of M with increasing N for both lattices. Note that N_s as well as M is independent of i .

We observe the convergence and reach the accuracy of six significant digits for $\sim 10^9$ particles in both lattices. This analysis confirms the usability of the AAEP to calculate the energy of even *ordered* structures. The accuracy may be improved still more with the increase of the single parameter—the number of ions N .

TABLE I. Madelung constant for bcc lattice calculated with Eq. (42) with increasing number of ions N . N_c denotes the number of primitive cells in the supercell, $N = 2N_c^3$. Exact: -0.8959293 .

N_c	N	$N_s - N$	M	Difference, %
1	2	-1	-0.8333856	-6.98088
3	54	5	-0.9036126	0.85759
4	128	9	-0.8998543	0.43810
8	1024	-59	-0.8941086	-0.20322
17	9826	15	-0.8956311	-0.03327
37	101 306	243	-0.8959880	0.00655
79	986 078	-543	-0.8959281	-0.00013
171	10 000 422	203	-0.8959254	-0.00043
369	100 486 818	763	-0.8959294	0.00002

B. Performance

It is of practical importance to compare the efficiency of computations between the exact Ewald formula and the AAEP. To demonstrate the calculation performance via the AAEP, we determine the Madelung constant of the bcc lattice for a different number of particles N in the supercell and measure the computational time. For comparison, we obtain M using the Ewald (6) and averaged (37) potentials. For the Ewald potential, we have taken into account several terms in the sum over \mathbf{n} with $n_x, n_y, n_z = -6, \dots, 6$. All the calculations were sequential and performed with a CPU Intel Core i7-7700HQ 2.8 GHz. The results are shown in Fig. 1. Both time dependencies are linear as N increases. The ratio of the slopes is ≈ 230 ; it means that the calculation of M is 230 times faster with the AAEP than with the Ewald potential. In addition, $v^a(r)$ is independent of any external parameters. This makes it a perspective tool for numerical simulations of Coulomb systems.

The calculation of the sum $\sum_{\substack{j=1 \\ j \neq i}}^{N_s} \tilde{v}(r_{ij})$ in Eq. (38) can be parallelized. We simply distribute the terms of this sum over various processes during an MC simulation, which allows us to effectively speed up the computation. A similar approach was considered in [54] for TCP calculations.

Next, we perform MC simulations of the OCP in a wide range of parameter Γ . We demonstrate the possibility of a simulation with *1 million particles* in the supercell.

TABLE II. Madelung constant for fcc lattice calculated with Eq. (42) with increasing number of ions N . N_c denotes the number of primitive cells in the supercell, $N = 4N_c^3$. Exact: -0.8958736 .

N_c	N	$N_s - N$	M	Difference, %
1	4	-3	-0.8504467	-5.07068
2	32	11	-0.8971610	0.14370
4	256	-7	-0.8947975	-0.12012
8	2048	45	-0.8962085	0.03738
17	19 652	-175	-0.8957744	-0.01107
37	202 612	89	-0.8958525	-0.00235
79	1 972 156	-169	-0.8958673	-0.00070
171	20 000 844	-207	-0.8958733	-0.00003
369	200 973 636	505	-0.8958739	0.00003

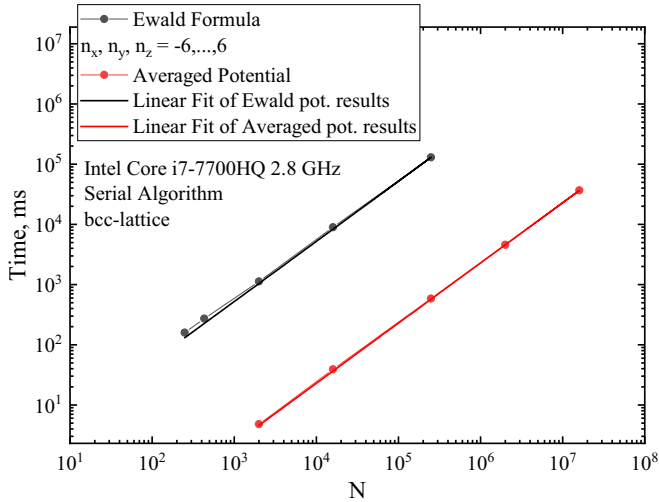


FIG. 1. Calculation time of the Madelung constant for a bcc lattice as a function of N . Both methods are linear in N ; the calculation with the AAEP is 230 times faster than with the Ewald potential. The slope of the curve obtained with the Ewald potential is 0.521 ms; that obtained with the averaged one is 2.39×10^{-3} ms.

C. MC simulations

We performed MC simulations using (38) for $\Gamma = 0.01, 0.05, 0.1, 1, 10, 100$. We demonstrate the capabilities of the AAEP using a *million* particles in a simulation cell for $\Gamma = 0.01-1$. Such an amount of particles is important since the Debye length $\lambda_D = 1/\sqrt{3\Gamma}$ diverges as $\Gamma \rightarrow 0$. Also, to obtain a reliable thermodynamic limit, it is necessary to know the value of energy at a significantly large N . Therefore one should consider a large simulation cell to obtain correct data.

A very good description of a MC simulation procedure can be found in [8, Sec. IV] and [68, Chapter 5]. Here we briefly describe the algorithm that we used.

We start from an initial ion configuration of N particles in a cubic supercell with random positions and calculate its energy U_{init} with Eq. (38). Then some ion i at a position \mathbf{r}_i is randomly chosen. Next, we calculate the potential $u(\mathbf{r}_i) = \sum_{\substack{j=1 \\ j \neq i}}^{N_s, i} \tilde{v}(r_{ij})$ at a point \mathbf{r}_i created by other particles (in the sphere of radius r_m). Now, this particle is moved as it is described in [8] producing a new ion position \mathbf{r}'_i . Again, we calculate the potential energy $u(\mathbf{r}'_i)$ and the total change in energy $\Delta U = [u(\mathbf{r}'_i) - u(\mathbf{r}_i)]\Gamma$. This trial move is accepted according to the Metropolis *et al.* algorithm [69] as is described in [8]. Now we have a new ionic configuration with energy $U_{\text{init}} + \Delta U$; some ion is randomly selected again and the whole procedure repeats itself. Thus, we obtain a sequence $U(m)$, where m denotes the ionic configuration number (or the trial move number). During the simulation we maintain the acceptance rate near 50% (if it is possible) according to Algorithm 5.1 in [68]. It is stated in [68, Sec. 5.1.2, p. 192] that such an algorithm increases the efficiency of a simulation.

Since we start from a randomly distributed ions position, which is not an equilibrium ionic configuration for a given Γ and N , we need to discard the starting section of the simulation. After reaching the equilibrium, we perform $m_{\text{tot}} = 10^7$ steps for $N = 10^2, 10^3, 10^4, 10^5, 10^6$

TABLE III. Parameters of MC simulations with AAEP.

Γ	N	m_{tot}	n_b
0.01	$10^2, 10^3, 10^4, 5 \times 10^4, 10^5, 10^6$	10^7	5
0.05	$10^2, 10^3, 10^4, 10^5, 10^6$	10^7	5
0.1	$10^2, 10^3, 10^4, 10^5, 10^6$	10^7	5
1	$10^2, 10^3, 10^4, 10^5, 10^6$	10^7	5
10	$10^2, 10^3, 10^4, 10^5$	10^8	50
100	$10^2, 150, 10^3, 10^4, 10^5$	10^8	50

at $\Gamma = 0.01, 0.05, 0.1, 1$. To decrease the statistical error, at $\Gamma = 10, 100$ we performed $m_{\text{tot}} = 10^8$ MC steps with $N = 10^2-10^5$. We also had to perform simulations for $N = 150, \Gamma = 100$ because the result for $N = 100$ is out of normal dependence [see Fig. 4(d) below]. As only large enough N can be used in a low- Γ regime, we performed simulation for $N = 5 \times 10^4$ and $\Gamma = 0.01$. All the simulation parameters are collected in Table III.

To calculate the averaged energy value and its statistical error, we use the standard block averaging [70, Chapter 11.4]. The entire equilibrium section is divided into several n_b blocks (see Fig. 2). Each such block contains $m_{\text{tot}}/n_b = 2 \times 10^6$ values of energy. We calculate an average energy value for each block, obtaining n_b energy values $\bar{U}(l)$. The average energy value U/N is calculated as the average of $\bar{U}(l)$. The statistical error σ is estimated as the root of the variance of these mean values:

$$\sigma = \sqrt{\frac{1}{n_b - 1} \sum_{l=1}^{n_b} \left(\frac{\bar{U}(l)}{N} - \frac{U}{N} \right)^2}. \quad (43)$$

To obtain the energy in the limit $N \rightarrow \infty$, which is often called the thermodynamic limit, we fit the dependence U/N on $1/N$ and evaluate the limit as $1/N \rightarrow 0$. In [7,26] it is stated that with $N \rightarrow \infty$, the dependence $U/N(1/N)$ has the

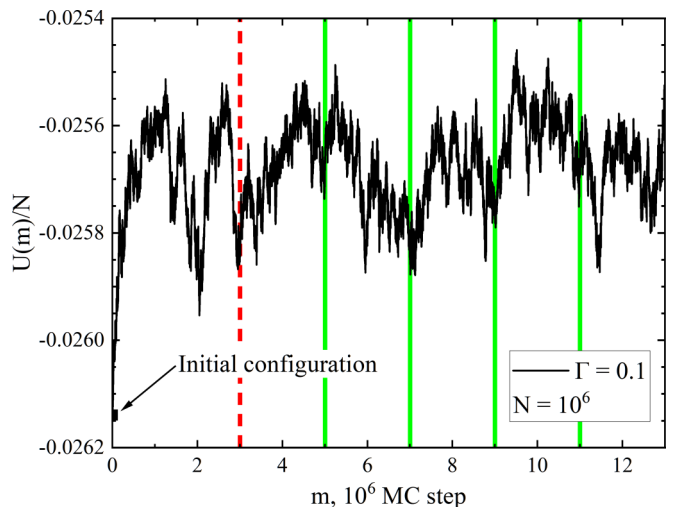


FIG. 2. OCP energy dependence $U(m)/N$ with 10^6 particles at $\Gamma = 0.1$. The vertical dashed red line shows the beginning of the equilibrium section. Green solid vertical lines show the partitioning of the equilibrium section into blocks.

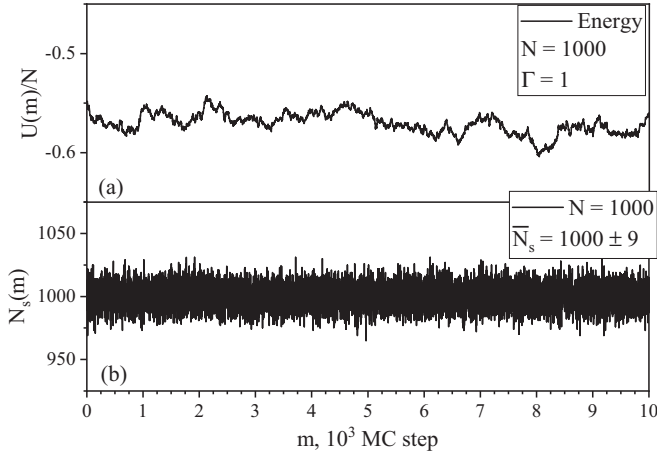


FIG. 3. The number of ions in a spherical cell and energy on the equilibrium section of MC simulation, $N = 10^3$, $\Gamma = 1$. (a) Energy; (b) number of ions in a spherical cell.

following form:

$$\frac{U}{N}(1/N) - \frac{U}{N}(0) \sim (1/N)^{2/3}, \quad \Gamma \rightarrow 0. \quad (44)$$

For $\Gamma \gg 1$ the authors of [7,26] use a linear fit $U/N(1/N) = U/N(0) + b(1/N)$ and a quadratic analog. In our work we use the following fitting function for all Γ and N :

$$\frac{U}{N}(1/N) = \frac{U}{N}(0) + b(1/N)^\gamma. \quad (45)$$

The values $U/N(0)$, b , γ are obtained from the fitting. We do not provide any theoretical background for this approximation; nevertheless, it works well. The obtained values of $U/N(0)$ are shown in Table IV.

Also, we perform simulations with the traditional Ewald potential (6) generating $m_{\text{tot}} = 10^7$ configurations for all $\Gamma = 0.1-100$ and $N = 10^2-10^4$ to compare. Only the terms with $n_x, n_y, n_z = -6, \dots, 6$ are taken into account during the calculation of the sum over \mathbf{n} in Eq. (8). The results are presented in Table V and in Fig. 4 below.

It is not difficult to reach the equilibrium section with $N \leq 10^5$. For one million particles, we used the following technique to speed up this simulation stage.

TABLE IV. Thermodynamic limit of MC results for $-U/N$ at $\Gamma = 0.01, 0.05, 0.1, 1, 10, 100$. The results obtained using the AAEP agree very well with Caillol *et al.* at $\Gamma = 1$, and with the theoretical values at $\Gamma = 0.01-0.1$. At $\Gamma = 10, 100$ we observe a small difference compared to [26]. The third row represents the thermodynamic limit of data from [26] obtained by Eq. (45). The digits in parentheses correspond to one standard deviation.

Γ	0.01	0.05	0.1	1	10	100
MC (AAEP, this work)	0.000 8611(42) ^a	0.009 395(13)	0.025 6975(35)	0.571 414(24)	7.998 170(16)	87.523 82(55)
MC (Caillol <i>et al.</i> [7,26])	—	—	0.025 127(34)	0.571 403(22)	7.997 974(45)	87.526 93(24)
Caillol's data, fit (45)	—	—	—	0.571 654(88)	7.997 996(39)	87.524 42(75)
Ortner [44, Eq. (94)]	0.000 861 93	0.009 386	0.025 699 174	1.665 188	—	—
Debye-Hückel, $\sqrt{3}\Gamma^{3/2}/2$	0.000 866 03	0.009 682	0.027 386 128	0.866 025	—	—
HNC	0.000 861 98 ^b	0.009 387 ^b	0.025 688 548	0.570 45534	—	—

^aOnly $N \geq 10^4$ were used for fitting (45).

^bObtained from HNC fit [7, Table 1].

To reach equilibrium with $N = 10^6$, we generated the initial configuration as follows. We performed an additional simulation for a small cell with $N = 15\,625$ to obtain one equilibrium configuration. Then we constructed a larger cell consisting of 2^3 small cells, which resulted in an intermediate cell of $N = 125\,000$ ions. Repeating this procedure, we got an initial cell with $N = 10^6$ particles; it consisted of $2^6 = 64$ identical small cells with $N = 15\,625$. Nevertheless, the equilibration process required quite a long simulation. We provide a graph of $U(m)$ for $\Gamma = 0.1$ and $N = 10^6$ (Fig. 2). One can see that at least $\sim 10^6$ steps should be discarded. We discarded 3×10^6 first steps.

V. RESULTS AND DISCUSSION

First, we consider the number of interactions during MC simulation. As we mentioned earlier, the number of ions N_s in the sphere around a chosen ion can be different from N . Let $N_s(m)$ be the number of ions in a sphere with the center at a randomly chosen ion at its initial position; here m is the trial move number. It turns out that the average number $\bar{N}_s = \frac{1}{m_{\text{tot}}} \sum_{m=1}^{m_{\text{tot}}} N_s(m)$ during MC simulations is close to N . The dependencies of $N_s(m)$ and $U(m)$ on the equilibrium section are shown in Fig. 3 for a simulation with $N = 10^3$, $\Gamma = 1$. In this simulation, $\bar{N}_s = (1.000 \pm 0.009) \times 10^3$ is close to $N = 10^3$.

We obtained a numerical dependence of energy U/N on the number of ions N for $0.01 \leq \Gamma \leq 100$ (see Table VI). To calculate the thermodynamic limit, we use Eq. (45). The results of our MC simulations and fitted curves are present in Table VI and Fig. 4.

Paper [7] gives the OCP energy values for $\Gamma = 0.1, 1$ obtained by solving the HNC integral equation; this method was outlined in [46]. According to [7], it is the most accurate theoretical result for the OCP energy in a low- Γ regime. In such a regime the Ortner Γ expansion [44] gives quite accurate results. For comparison, we provide MC results from [7,26] and obtained with the Ewald potential (5). The digits in parentheses correspond to one standard deviation.

Approximation (45) quite accurately describes the dependence on $1/N$ over a wide range of N and Γ , which varies by several orders of magnitude. However, for unknown reasons, at $\Gamma = 100$, the point $N = 100$ is out of dependence. This point was excluded from the fitting procedure.

TABLE V. MC results for $-U^{\text{Ew}}/N$ at $\Gamma = 0.1, 1, 10, 100$ as a function of N using the Ewald potential (5), $n_x, n_y, n_z = -6, \dots, 6$. The digits in parentheses correspond to one standard deviation.

$\Gamma \backslash N$	10^2	150	10^3	10^4
0.1	0.029815(34)	—	0.026178(61)	0.025737(35)
1	0.57646(21)	—	0.57197(24)	0.57153(28)
10	8.0031(11)	—	7.99955(70)	7.9977(12)
100	87.5327(77)	87.524(12)	87.5278(77)	87.5208(45)

TABLE VI. MC results for $-U/N$ at $\Gamma = 0.1, 1, 10, 100$ as a function of N using the AAEP. The digits in parentheses correspond to one standard deviation.

$\Gamma \backslash N$	10^2	150	10^3	10^4	5×10^4	10^5	10^6
0.01	0.0020724(45)	—	0.0011814(96)	0.000917(12)	0.000875(11)	0.000866(15)	0.000863(14)
0.05	0.012662(30)	—	0.009855(38)	0.009439(31)	—	0.009405(54)	0.009409(31)
0.1	0.029951(50)	—	0.026144(11)	0.025756(63)	—	0.025704(21)	0.025691(37)
1	0.57682(21)	—	0.57201(15)	0.57144(21)	—	0.57149(34)	0.57142(14)
10	8.0043(14)	—	7.9985(13)	7.9982(14)	—	7.9982(14)	—
100	87.485(11)	87.645(11)	87.5295(62)	87.5248(50)	—	87.5235(33)	—

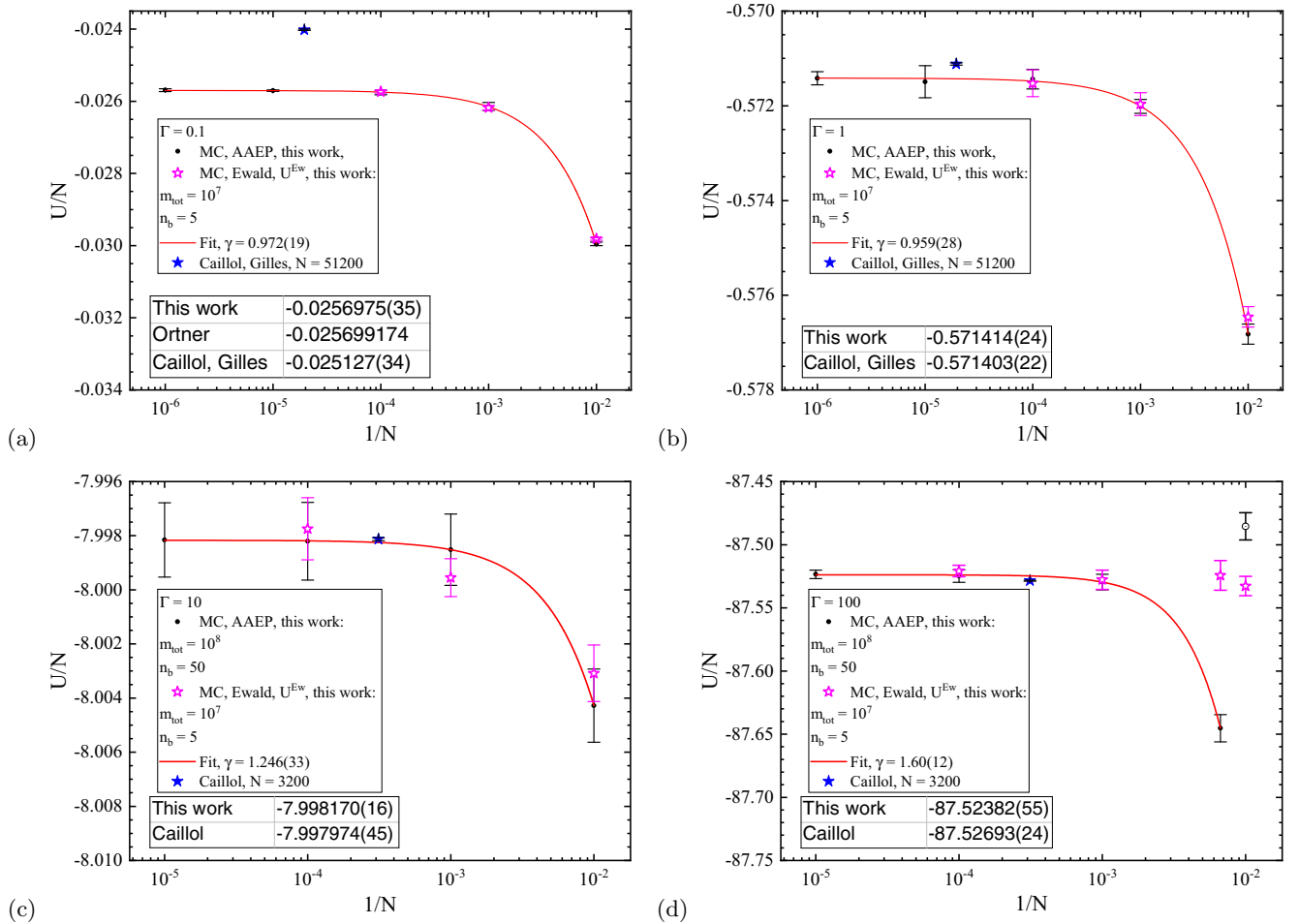


FIG. 4. Results of MC simulations at $\Gamma = 0.1, 1, 10, 100$ (points with bars) together with the numerical fit (45) (solid lines). Error bars are calculated with Eq. (43). Thermodynamic limit energy values from [7,26] are shown for comparison. Blue stars represent MC data for the largest N in [7,26]. Purple stars correspond to our MC simulations with the Ewald potential (5). Digits in parentheses correspond to one standard deviation.

At $\Gamma \leq 1$, the power-law index changes weakly and is close to $\gamma = 1$. As Γ increases, the index γ also increases.

From approximation (45), we find energy values in the thermodynamic limit as $1/N \rightarrow 0$. Table IV presents the results of our extrapolation in comparison with the MC, HNC results by Caillol *et al.* [7,26], and the Ortner expression [44, Eq. (94)]. For $\Gamma = 1$, our result is the same as that of Caillol *et al.* In the case of $\Gamma = 0.01-0.1$, our result coincides with the HNC and Ortner values. It speaks in favor of our method in comparison to MC of [7]. In the case of $\Gamma = 10$ and $\Gamma = 100$, we observe a difference of $2 \times 10^{-3}\%$ and $4 \times 10^{-3}\%$, respectively, from the Caillol result, which exceeds the statistical error.

We fitted the Caillol [26] MC data by Eq. (45); the result is presented in Table IV (third row). We observe, that for $\Gamma = 1, 100$ the energy value significantly changes. In contrast to the original Caillol result, these values coincide with ours at $\Gamma = 100$ and differ at $\Gamma = 1$. So the thermodynamic limit depends on the fitting function. Let us note that Caillol used different fitting functions at various Γ (see Table II in [26]). The extrapolation $1/N \rightarrow 0$ with different dependencies on N at various Γ is a disadvantage of [26]. In our paper, only one extrapolation dependence (45) is used.

In Fig. 4 we provide the MC data for the largest N in [7,26] (blue stars). Despite the fact that λ_D^3 is much less than the system volume, we believe that for the stated accuracy $N = 3200$ is not enough. This circumstance may increase the final error in [26].

The results of MC simulations via the Ewald potential are presented in Table V and in Fig. 4 (purple stars). One can see that the traditional Ewald simulation and the one via the AAEP give close results for $N \geq 10^3$. At the same time, at $N = 10^2$ there are differences; the biggest one is for $\Gamma = 100$.

We calculate the RDF, $g(r)$, from MC simulations via the traditional Ewald potential (5) and the AAEP (38) for $\Gamma = 0.1, 1, 10, 100$ and $N = 10^4$. The results are represented in Fig. 5. For the calculation of $g(r)$ 10^4 configurations are chosen from the MC chain. The curves obtained by both methods coincide with each other for all Γ .

At $\Gamma = 100$ and $N = 10^2$ we observe differences in $g(r)$ starting from the second maximum (see Fig. 4). This behavior causes the difference in energy between the exact and angular-averaged Ewald potential. Nevertheless, both functions for $\Gamma = 100, N = 10^2$ are shifted from the correct $g(r)$. If the N convergence is observed, the RDFs obtained with the Ewald and AAEP potentials coincide.

Thus, we demonstrate the applicability and high accuracy of the OCP AAEP for the calculation of energy in the broad range of the Γ parameter. Also, the AAEP shows impressive effectiveness in comparison with the exact Ewald potential. Unfortunately, it is not possible to make a direct performance comparison with the works [7,26]. In Ref. [7] it is stated that they require ‘‘one month for 10 000 configurations’’ for $N = 51\,200$. In our study, we generated 10^7 configurations in 46 h and in 3 wk for $N = 10^5$ and $N = 10^6$, respectively. This means that a similar calculation for $N = 50\,000$ and 10^4 MC steps would take $46/2/10^7 \times 10^4 = 0.023$ h. Thus we estimate that the speed of our calculation is about 30 thousand times greater than in [7]. Due to this fact the AAEP can be applied to a very large number of particles in a supercell.

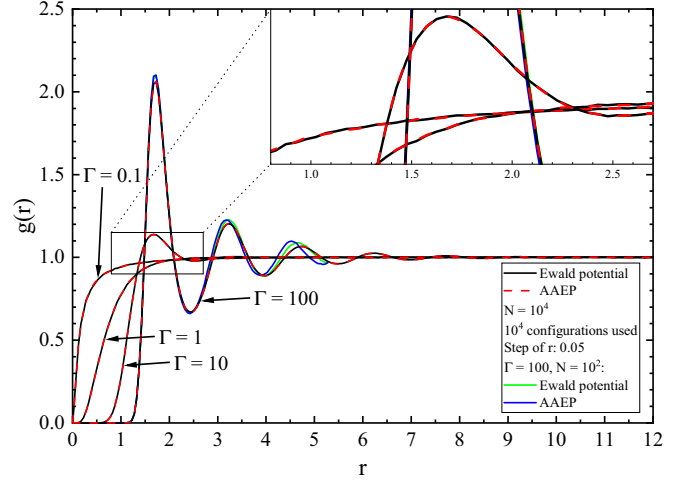


FIG. 5. RDF, $g(r)$, calculated from MC simulations via the traditional Ewald potential (5) (black solid line) and the AAEP (38) (red dash line) for $\Gamma = 0.1, 1, 10, 100$ and $N = 10^4$. Only 10^4 configurations are used to calculate $g(r)$. The calculations via both methods agree very well. Green and blue lines represent $g(r)$ for $\Gamma = 100, N = 10^2$ computed with both potentials; a significant difference is observed.

We believe that the OCP energy can be calculated with this method to refine and verify previous results for the OCP.

VI. CONCLUSION

A correct expression for the angular-averaged Ewald potential (AAEP) in an OCP was obtained. For this purpose we considered an exact anisotropic Ewald potential introduced especially for an OCP and constructed the power series of the angular-averaged potential. Using the Fourier transform, Taylor expansion, and Poisson formula, we rigorously demonstrated that all coefficients of the power series are identically zero except for the first two. Then with the cluster expansion in the limit $\Gamma \rightarrow 0$ we corrected the potential to avoid the divergence of potential energy. Finally, we shifted the potential so that the resulting AAEP completely vanished at $r > r_m$. We also derived the correct expression for the OCP energy expressed through the AAEP. With the correct expression for the AAEP, it was shown that the same expression for the OCP energy can be obtained from the TCP energy.

Our calculations of the Madelung constant demonstrated that the AAEP turned out to be about 230 times more effective than the original Ewald potential at a comparable accuracy. We also performed OCP MC simulations in the range $0.01 \leq \Gamma \leq 100$ with up to a million particles in a computational cell. Our result at $\Gamma = 0.01-0.1$ is very close to the HNC [7] and Ortner [44] values. At $\Gamma = 1$ our MC data agree very well with Caillol *et al.* [7].

Thus, the AAEP turned out to be very effective and accurate in the simulations of classical Coulomb systems. We anticipate that the main advantage of the AAEP will be shown in simulations of quantum systems such as jellium (uniform electron gas) or degenerate TCP [11–13].

ACKNOWLEDGMENTS

We thank Alexander Larkin for the idea of the OCP energy derivation from the expression for the TCP energy developed in Appendix C. The authors acknowledge the JIHT RAS Supercomputer Centre, the Joint Supercomputer Centre of the Russian Academy of Sciences, and the Shared Resource Centre “Far Eastern Computing Resource” IACP FEB RAS for providing computing time.

APPENDIX A: COEFFICIENTS OF TAYLOR EXPANSION

Our goal now is to obtain the coefficients of the Taylor expansion (17). A direct Taylor expansion of (16) can not be used, since we have the noncentral terms $f(n+x)$ and $f(n-x)$ [$f(x)$ is defined in Eq. (14)]. This difficulty complicates the derivation compared to a TCP [65, Eqs. (12), (13)], where these terms can be excluded.

Let us decompose $f(n+x)$ into a Fourier integral of the variable n :

$$f(n+x) = \int_{-\infty}^{+\infty} \mathcal{F}_n[f(x+n)](\omega) e^{-i\omega n} d\omega, \quad (\text{A1})$$

where $\mathcal{F}_n[f(n)](\omega)$ is a Fourier transform:

$$\mathcal{F}_n[f(n)](\omega) = \frac{1}{2\pi} \int_{-\infty}^{+\infty} f(n) e^{i\omega n} dn. \quad (\text{A2})$$

Using the following property of the Fourier transform:

$$\mathcal{F}_n[f(x+n)](\omega) = e^{-i\omega x} \mathcal{F}_n[f(n)](\omega), \quad (\text{A3})$$

we get

$$f(n+x) = \int_{-\infty}^{+\infty} e^{-i\omega x} \mathcal{F}_n[f(n)](\omega) e^{-i\omega n} d\omega. \quad (\text{A4})$$

Thus, expression $f(n-x) - f(n+x)$ transforms into

$$f(n-x) - f(n+x) = 2i \int_{-\infty}^{+\infty} \mathcal{F}_n[f(n)](\omega) \sin(\omega x) e^{-i\omega n} d\omega. \quad (\text{A5})$$

Now we can expand $\sin(\omega x)$ into the Taylor series at $x=0$:

$$f(n-x) - f(n+x) = \sum_{k=0}^{\infty} \left(2i \int_{-\infty}^{+\infty} \mathcal{F}_n[f(n)](\omega) \frac{(-1)^k \omega^{2k+1}}{(2k+1)!} e^{-i\omega n} d\omega \right) x^{2k+1}, \quad (\text{A6})$$

or, using the inverse Fourier transform notation, we rewrite Eq. (A6):

$$f(n-x) - f(n+x) = \sum_{k=0}^{\infty} \frac{2i(-1)^k}{(2k+1)!} \mathcal{F}_\omega^{-1}[\omega^{2k+1} \mathcal{F}_n[f(n)](\omega)](n) x^{2k+1}. \quad (\text{A7})$$

The Fourier transform $\mathcal{F}_n[f(n)](\omega)$ is

$$\mathcal{F}_n[e^{-\pi n^2} - \pi n \operatorname{erfc}(\sqrt{\pi} n)] = -\frac{e^{-\frac{\omega^2}{4\pi}}}{\omega^2} + i\pi \delta'(\omega). \quad (\text{A8})$$

Since we multiply (A8) by ω^{2k+1} , the second term has zero impact for $k \geq 1$. Thus,

$$\mathcal{F}_\omega^{-1} \left[\omega^{2k+1} \left(-\frac{e^{-\frac{\omega^2}{4\pi}}}{\omega^2} \right) \right] (n) = i 2^{1+2k} \pi^{k+\frac{1}{2}} n \Gamma\left(k + \frac{1}{2}\right) e^{-\pi n^2} M\left(1-k, \frac{3}{2}, n^2 \pi\right), \quad (\text{A9})$$

where $M(a, b, x)$ is the confluent hypergeometric function defined by the series

$$M(a, b, x) = \sum_{s=1}^{\infty} \frac{a^{(s)}}{b^{(s)} s!} x^s, \quad (\text{A10})$$

where $a^{(s)}$ denotes the rising factorial:

$$a^{(0)} = 1, a^{(s)} = a(a+1)(a+2) \cdots (a+s-1). \quad (\text{A11})$$

Also, $\Gamma(k)$ identifies the Γ function. Then, expanding $\sin(2\pi n x)$ in Eq. (16) at $x=0$, we obtain for the second part of the pair AAEP $v_2^a(x)$ the following formula:

$$Lv_2^a(x) = (3 - C_0) + \sum_{k=1}^{\infty} (-1)^k \sum_{n \neq 0} e^{-\pi n^2} \left[-\frac{2^{1+2k} \pi^{k-\frac{1}{2}}}{(2k+1)!} \Gamma\left(k + \frac{1}{2}\right) M\left(1-k, \frac{3}{2}, n^2 \pi\right) + \frac{2^{2k} \pi^{2k-1} n^{2k-2}}{(2k+1)!} \right] x^{2k}. \quad (\text{A12})$$

Expanding the erfc function at $x=0$ in Eq. (7), we get the expression for C_k in Eq. (17) (if $k \geq 1$):

$$C_k = (-1)^k \sum_{n \neq 0} e^{-\pi n^2} \left[\frac{2^{2k} \pi^{2k-1} n^{2k-2}}{(2k+1)!} - \frac{2^{1+2k} \pi^{k-\frac{1}{2}}}{(2k+1)!} \Gamma\left(k + \frac{1}{2}\right) M\left(1-k, \frac{3}{2}, n^2 \pi\right) \right] - \frac{2(-1)^k \pi^k}{(2k+1)k!}. \quad (\text{A13})$$

By adding and subtracting the contribution at $\mathbf{n} = \mathbf{0}$ and using the Γ function property $\Gamma(k + 1/2) = (2k)! \sqrt{\pi} / (2^{2k} k!)$, we get the final expression for C_k :

$$C_k = (-1)^k \sum_{\mathbf{n}} e^{-\pi n^2} \left[\frac{2^{2k} \pi^{2k-1} n^{2k-2}}{(2k+1)!} - \frac{2^{1+2k} \pi^{k-\frac{1}{2}}}{(2k+1)!} \Gamma\left(k + \frac{1}{2}\right) M\left(1 - k, \frac{3}{2}, n^2 \pi\right) \right] + \frac{2\pi}{3} \delta_{1,k}, \quad k \geq 1, \quad (\text{A14})$$

where $\delta_{1,k}$ is the Kronecker symbol.

APPENDIX B: ZEROING THE COEFFICIENTS

We are going to prove the equality

$$\begin{aligned} & \frac{2^{2k} \pi^{2k-1}}{(2k+1)!} \sum_{\mathbf{n}} e^{-\pi n^2} n^{2k-2} \\ &= \frac{2^{1+2k} \pi^{k-\frac{1}{2}}}{(2k+1)!} \Gamma\left(k + \frac{1}{2}\right) \sum_{\mathbf{n}} e^{-\pi n^2} M\left(1 - k, \frac{3}{2}, n^2 \pi\right), \end{aligned} \quad (\text{B1})$$

from which it follows that $C_k = 0$ for $k \geq 2$. To do this, we use the Poisson formula:

$$\sum_{\mathbf{n}} e^{-\pi n^2} n^{2k-2} = \sum_{\mathbf{q}} F_k(\mathbf{q}), \quad (\text{B2})$$

where

$$\begin{aligned} F_k(\mathbf{q}) &= \int e^{-\pi n^2} n^{2k-2} e^{-2\pi i \mathbf{n} \cdot \mathbf{q}} d^3 n \\ &= 2\pi^{\frac{1}{2}-k} \Gamma\left(k + \frac{1}{2}\right) e^{-\pi q^2} M\left(1 - k, \frac{3}{2}, q^2 \pi\right) \end{aligned} \quad (\text{B3})$$

is a Fourier transform. Substituting (B3) in the left-hand side of Eq. (B1) turns Eq. (B1) into an identity. Thus, $C_k = 0$ for $k \geq 2$.

APPENDIX C: DERIVATION OF THE OCP AAEP FROM THE TCP ONE

In Refs. [52], [65, Eq. (59)] the energy of TCP was obtained by the angular averaging of the TCP Ewald potential. We consider a plasma with two sorts of particles with charges $Q_+ = +Ze$ and $Q_- = -Ze$. Then the internal energy reads

$$\frac{U}{\Gamma} = - \sum_{i=1}^N \frac{3z_i^2}{4r_m} + \frac{1}{2} \sum_{i=1}^N z_i \sum_{\substack{j=1 \\ j \neq i}}^N z_j \tilde{v}(r_{ij}). \quad (\text{C1})$$

Here $\Gamma = (Ze)^2 / (k_B T a)$, z_i is a charge *sign* and $\tilde{v}(r)$ is defined by Eq. (37). Below we obtain Eq. (38) for the OCP energy from Eq. (C1). The main idea is to separate the summation in Eq. (C1) for positive and negative ions; then consider a transition from the summation over point charges to the integration over a uniformly distributed charge.

We separate positive and negative ions:

$$N = N_+ + N_- = 2N_+ = 2N_-, \quad (\text{C2})$$

where N_+ and N_- denote the number of positive and negative ions, respectively. Let us consider the first term in Eq. (C1):

$$- \sum_{i=1}^N \frac{3z_i^2}{4r_m} = - \sum_{i=1}^{N_-} \frac{3z_i^2}{4r_m} - \sum_{i=1}^{N_+} \frac{3z_i^2}{4r_m}. \quad (\text{C3})$$

For positive ions, we keep this term as a discrete sum with $z_i = 1$:

$$- \sum_{i=1}^{N_+} \frac{3z_i^2}{4r_m} = - \frac{3N_+}{4r_m}. \quad (\text{C4})$$

Now we consider each negative ion as a space element with an infinitesimal charge

$$z_i \rightarrow -\rho dV, \quad (\text{C5})$$

where $\rho = N_+ / L^3 = N_- / L^3$ is the *number density* and dV denotes a space element. Then we replace the summation over negative charges with an integral over space:

$$\sum_{i=1}^{N_-} z_i \rightarrow - \int \rho dV. \quad (\text{C6})$$

The first term in Eq. (C3) contains z_i^2 , while the summation is performed once. As we proceed to integration, this term has an infinitesimal contribution to the energy of the system:

$$- \sum_{i=1}^{N_-} \frac{3z_i^2}{4r_m} \rightarrow 0. \quad (\text{C7})$$

Next, we consider the two-particle contribution to the energy. This term results in three sums:

$$\begin{aligned} \sum_{i=1}^N z_i \sum_{\substack{j=1 \\ j \neq i}}^N z_j \tilde{v}(r_{ij}) &= \sum_{i=1}^{N_-} z_i \sum_{\substack{j=1 \\ j \neq i}}^{N_-} z_j \tilde{v}(r_{ij}) + 2 \sum_{i=1}^{N_+} z_i \sum_{j=1}^{N_-} z_j \tilde{v}(r_{ij}) \\ &+ \sum_{i=1}^{N_+} z_i \sum_{\substack{j=1 \\ j \neq i}}^{N_+} z_j \tilde{v}(r_{ij}). \end{aligned} \quad (\text{C8})$$

The last term in Eq. (C8) remains unchanged. We change the second term into the integral over space:

$$\begin{aligned} 2 \sum_{i=1}^{N_+} z_i \sum_{j=1}^{N_-} z_j \tilde{v}(r_{ij}) &\rightarrow -2 \sum_{i=1}^{N_+} z_i \int \rho \tilde{v}(|\mathbf{r}_j - \mathbf{r}_i|) d\mathbf{r}_j \\ &= -2 \sum_{i=1}^{N_+} z_i \int \rho \tilde{v}(|\mathbf{r}_j - \mathbf{r}_i|) d(\mathbf{r}_j - \mathbf{r}_i) \\ &= -2 \sum_{i=1}^{N_+} z_i \int \rho \tilde{v}(u) d\mathbf{u}, \end{aligned} \quad (\text{C9})$$

where $\mathbf{u} = \mathbf{r}_j - \mathbf{r}_i$. We calculate this integral in spherical coordinates:

$$\begin{aligned} -2 \sum_{i=1}^{N_+} z_i \int \rho \tilde{v}(u) d\mathbf{u} &= -2 \sum_{i=1}^{N_+} z_i \int_0^{r_m} 4\pi u^2 \rho \tilde{v}(u) du \\ &= -2N_+ 4\pi \rho r_m^2 \frac{1}{10}. \end{aligned} \quad (\text{C10})$$

Since

$$\rho = \frac{N_+}{L^3} = \frac{N_+}{\frac{4\pi}{3} r_m^3}, \quad (\text{C11})$$

we obtain the expression

$$2 \sum_{i=1}^{N_+} z_i \sum_{j=1}^{N_-} z_j \tilde{v}(r_{ij}) \rightarrow -\frac{6}{10} \frac{N_+^2}{r_m}. \quad (\text{C12})$$

The first term in Eq. (C8) is also replaced with an integral:

$$\sum_{i=1}^{N_-} z_i \sum_{\substack{j=1 \\ j \neq i}}^{N_-} z_j \tilde{v}(r_{ij}) \rightarrow -\sum_{i=1}^{N_-} z_i 4\pi \rho \int_0^{r_m} u^2 \tilde{v}(u) du. \quad (\text{C13})$$

We calculate this integral and get

$$-\sum_{i=1}^{N_-} z_i 4\pi \rho r_m^2 / 10. \quad (\text{C14})$$

This sum also should be integrated. Since the integrand is constant, we obtain

$$-\sum_{i=1}^{N_-} z_i 4\pi \rho r_m^2 / 10 \rightarrow \rho \times \frac{4\pi}{3} r_m^3 \times 4\pi \rho r_m^2 / 10. \quad (\text{C15})$$

Using Eq. (C11), we get

$$\sum_{i=1}^{N_-} z_i \sum_{\substack{j=1 \\ j \neq i}}^{N_-} z_j \phi(r_{ij}) \rightarrow \frac{3}{10} \frac{N_-^2}{r_m} = \frac{3}{10} \frac{N_+^2}{r_m}. \quad (\text{C16})$$

Substituting Eqs. (C4), (C7), (C8), (C12), and (C16) in (C1), we get the OCP energy:

$$\begin{aligned} \frac{U}{\Gamma} &= -\frac{3N_+}{4r_m} - \frac{1}{2} \frac{6}{10} \frac{N_+^2}{r_m} + \frac{1}{2} \frac{3}{10} \frac{N_+^2}{r_m} + \frac{1}{2} \sum_{i=1}^{N_+} \sum_{\substack{j=1 \\ j \neq i}}^{N_+} \tilde{v}(r_{ij}) \\ &= -\frac{3}{20} \frac{N_+(N_+ + 5)}{r_m} + \frac{1}{2} \sum_{i=1}^{N_+} \sum_{\substack{j=1 \\ j \neq i}}^{N_+} \tilde{v}(r_{ij}). \end{aligned} \quad (\text{C17})$$

This expression is the same as Eq. (38) obtained from the OCP AAEP.

-
- [1] J. P. Hansen, Statistical mechanics of dense ionized matter. I. Equilibrium properties of the classical one-component plasma, *Phys. Rev. A* **8**, 3096 (1973).
- [2] W. L. Slattery, G. D. Doolen, and H. E. DeWitt, Improved equation of state for the classical one-component plasma, *Phys. Rev. A* **21**, 2087 (1980).
- [3] M. Baus and J.-P. Hansen, Statistical mechanics of simple Coulomb systems, *Phys. Rep.* **59**, 1 (1980).
- [4] G. S. Stringfellow, H. E. DeWitt, and W. L. Slattery, Equation of state of the one-component plasma derived from precision Monte Carlo calculations, *Phys. Rev. A* **41**, 1105 (1990).
- [5] A. Y. Potekhin and G. Chabrier, Equation of state of fully ionized electron-ion plasmas. II. Extension to relativistic densities and to the solid phase, *Phys. Rev. E* **62**, 8554 (2000).
- [6] S. A. Khrapak and A. G. Khrapak, Simple thermodynamics of strongly coupled one-component-plasma in two and three dimensions, *Phys. Plasmas* **21**, 104505 (2014).
- [7] J.-M. Caillol and D. Gilles, An accurate equation of state for the one-component plasma in the low coupling regime, *J. Phys. A: Math. Theor.* **43**, 105501 (2010).
- [8] S. G. Brush, H. L. Sahlin, and E. Teller, Monte Carlo study of a one-component plasma. I, *J. Chem. Phys.* **45**, 2102 (1966).
- [9] E. Wigner, Effects of the electron interaction on the energy levels of electrons in metals, *Trans. Faraday Soc.* **34**, 678 (1938).
- [10] T. Dornheim, S. Groth, and M. Bonitz, The uniform electron gas at warm dense matter conditions, *Phys. Rep.* **744**, 1 (2018).
- [11] V. S. Filinov, V. E. Fortov, M. Bonitz, and Z. Moldabekov, Fermionic path-integral Monte Carlo results for the uniform electron gas at finite temperature, *Phys. Rev. E* **91**, 033108 (2015).
- [12] T. Dornheim, Fermion sign problem in path integral Monte Carlo simulations: Quantum dots, ultracold atoms, and warm dense matter, *Phys. Rev. E* **100**, 023307 (2019).
- [13] T. Dornheim, S. Groth, A. V. Filinov, and M. Bonitz, Path integral Monte Carlo simulation of degenerate electrons: Permutation-cycle properties, *J. Chem. Phys.* **151**, 014108 (2019).
- [14] E. H. Lieb and H. Narnhofer, The thermodynamic limit for jellium, *J. Stat. Phys.* **12**, 291 (1975).
- [15] L. E. M. Landau L. D., *Statisticheskaya Fizika (Statistical Physics) Pt. 1* (Nauka, Moscow, 1976) [English translation (Oxford: Pergamon Press, 1980)].
- [16] F. Daan and S. Berend, *Understanding Molecular Simulation* (Academic Press, San Diego, 2001).

- [17] P. P. Ewald, Die Berechnung optischer und elektrostatischer Gitterpotentiale, *Ann. Phys.* **369**, 253 (1921).
- [18] T. Darden, D. York, and L. Pedersen, Particle mesh Ewald: An $N \cdot \log(N)$ method for Ewald sums in large systems, *J. Chem. Phys.* **98**, 10089 (1993).
- [19] U. Essmann, L. Perera, M. L. Berkowitz, T. Darden, H. Lee, and L. G. Pedersen, A smooth particle mesh Ewald method, *J. Chem. Phys.* **103**, 8577 (1995).
- [20] R. Hockney and J. Eastwood, *Computer Simulation Using Particles* (CRC Press, Boca Raton, FL, 2021).
- [21] W. L. Slattery, G. D. Doolen, and H. E. DeWitt, N dependence in the classical one-component plasma Monte Carlo calculations, *Phys. Rev. A* **26**, 2255 (1982).
- [22] S. Ogata and S. Ichimaru, Critical examination of N dependence in the Monte Carlo calculations for a classical one-component plasma, *Phys. Rev. A* **36**, 5451 (1987).
- [23] J. Caillol, Exact results for a two-dimensional one-component plasma on a sphere, *J. Phys. Lett.* **42**, 245 (1981).
- [24] J. M. Caillol, D. Levesque, J. J. Weis, and J. P. Hansen, A Monte Carlo study of the classical two-dimensional one-component plasma, *J. Stat. Phys.* **28**, 325 (1982).
- [25] J. M. Caillol, Numerical simulations of Coulomb systems: A comparison between hyperspherical and periodic boundary conditions, *J. Chem. Phys.* **111**, 6528 (1999).
- [26] J. M. Caillol, Thermodynamic limit of the excess internal energy of the fluid phase of a one-component plasma: A Monte Carlo study, *J. Chem. Phys.* **111**, 6538 (1999).
- [27] J.-M. Caillol, A symplectic integrator for molecular dynamics on a hypersphere, *Condens. Matter Phys.* **23**, 23603 (2020).
- [28] B. Scheiner and S. D. Baalrud, Testing thermal conductivity models with equilibrium molecular dynamics simulations of the one-component plasma, *Phys. Rev. E* **100**, 043206 (2019).
- [29] I. Korolov, G. J. Kalman, L. Silvestri, and Z. Donkó, The dynamical structure function of the one-component plasma revisited, *Contrib. Plasma Phys.* **55**, 421 (2015).
- [30] T. Ott and M. Bonitz, Diffusion in a Strongly Coupled Magnetized Plasma, *Phys. Rev. Lett.* **107**, 135003 (2011).
- [31] G. S. Dubey, G. Gumbs, and V. Fessatidis, Dynamical properties of magnetized two-dimensional one-component plasma, *Phys. Lett. A* **382**, 1374 (2018).
- [32] H. Kählert and M. Bonitz, Dynamic structure factor of the magnetized one-component plasma: Crossover from weak to strong coupling, *Phys. Rev. Research* **4**, 013197 (2022).
- [33] J. P. Hansen, E. L. Pollock, and I. R. McDonald, Velocity Autocorrelation Function and Dynamical Structure Factor of the Classical One-Component Plasma, *Phys. Rev. Lett.* **32**, 277 (1974).
- [34] J. P. Hansen, I. R. McDonald, and E. L. Pollock, Statistical mechanics of dense ionized matter. III. Dynamical properties of the classical one-component plasma, *Phys. Rev. A* **11**, 1025 (1975).
- [35] B. Bernu and P. Vieillefosse, Transport coefficients of the classical one-component plasma, *Phys. Rev. A* **18**, 2345 (1978).
- [36] R. T. Farouki and S. Hamaguchi, Thermal energy of the crystalline one-component plasma from dynamical simulations, *Phys. Rev. E* **47**, 4330 (1993).
- [37] Y. Ueshima, K. Nishihara, D. M. Barnett, T. Tajima, and H. Furukawa, Particle simulation of Lyapunov exponents in one-component strongly coupled plasmas, *Phys. Rev. E* **55**, 3439 (1997).
- [38] G. Salin and J.-M. Caillol, Equilibrium molecular dynamics simulations of the transport coefficients of the Yukawa one component plasma, *Phys. Plasmas* **10**, 1220 (2003).
- [39] T. Ott, H. Löwen, and M. Bonitz, Dynamics of two-dimensional one-component and binary Yukawa systems in a magnetic field, *Phys. Rev. E* **89**, 013105 (2014).
- [40] R. T. Farouki and S. Hamaguchi, Thermodynamics of strongly-coupled Yukawa systems near the one-component-plasma limit. II. Molecular dynamics simulations, *J. Chem. Phys.* **101**, 9885 (1994).
- [41] S. Hamaguchi and R. T. Farouki, Thermodynamics of strongly-coupled Yukawa systems near the one-component-plasma limit. I. Derivation of the excess energy, *J. Chem. Phys.* **101**, 9876 (1994).
- [42] P. Debye and E. Hückel, Zur Theorie der Elektrolyte, I. Gefrierpunktserniedrigung und verwandte Erscheinungen, *Phys. Z.* **9**, 185 (1923).
- [43] E. G. D. Cohen and T. J. Murphy, New results in the theory of the classical electron gas, *Phys. Fluids* **12**, 1404 (1969).
- [44] J. Ortner, Equation of states for classical Coulomb systems: Use of the Hubbard-Schofield approach, *Phys. Rev. E* **59**, 6312 (1999).
- [45] N. V. Brilliantov, Accurate first-principle equation of state for the one-component plasma, *Contrib. Plasma Phys.* **38**, 489 (1998).
- [46] K.-C. Ng, Hypernetted chain solutions for the classical one-component plasma up to $\Gamma=7000$, *J. Chem. Phys.* **61**, 2680 (1974).
- [47] F. L. Castello and P. Tolia, On the advanced integral equation theory description of dense Yukawa one-component plasma liquids, *Contrib. Plasma Phys.* **61**, e202000105 (2021).
- [48] P. Tolia, S. Ratynskaia, and U. de Angelis, Soft mean spherical approximation for dusty plasma liquids: One-component Yukawa systems with plasma shielding, *Phys. Rev. E* **90**, 053101 (2014).
- [49] F. J. Rogers, D. A. Young, H. E. DeWitt, and M. Ross, One-component plasma structure factor in tabular form, *Phys. Rev. A* **28**, 2990 (1983).
- [50] H. Iyetomi, S. Ogata, and S. Ichimaru, Bridge functions and improvement on the hypernetted-chain approximation for classical one-component plasmas, *Phys. Rev. A* **46**, 1051 (1992).
- [51] F. Lucco Castello and P. Tolia, Bridge functions of classical one-component plasmas, *Phys. Rev. E* **105**, 015208 (2022).
- [52] E. Yakub and C. Ronchi, An efficient method for computation of long-ranged Coulomb forces in computer simulation of ionic fluids, *J. Chem. Phys.* **119**, 11556 (2003).
- [53] E. Yakub, Effective computer simulation of strongly coupled Coulomb fluids, *J. Phys. A: Math. Gen.* **39**, 4643 (2006).
- [54] P. K. Jha, R. Sknepnek, G. I. Guerrero-García, and M. Olvera de la Cruz, A graphics processing unit implementation of Coulomb interaction in molecular dynamics, *J. Chem. Theory Comput.* **6**, 3058 (2010).
- [55] V. S. Filinov, A. S. Larkin, and P. R. Levashov, Uniform electron gas at finite temperature by fermionic-path-integral Monte Carlo simulations, *Phys. Rev. E* **102**, 033203 (2020).
- [56] E. Yakub, C. Ronchi, and D. Staicu, Molecular dynamics simulation of premelting and melting phase transitions in stoichiometric uranium dioxide, *J. Chem. Phys.* **127**, 094508 (2007).

- [57] I. Fukuda, Y. Yonezawa, and H. Nakamura, Molecular dynamics scheme for precise estimation of electrostatic interaction via zero-dipole summation principle, *J. Chem. Phys.* **134**, 164107 (2011).
- [58] I. Fukuda and H. Nakamura, Non-Ewald methods: Theory and applications to molecular systems, *Biophys. Rev.* **4**, 161 (2012).
- [59] G. I. Guerrero-García, P. González-Mozuelos, and M. Olvera de la Cruz, Potential of mean force between identical charged nanoparticles immersed in a size-asymmetric monovalent electrolyte, *J. Chem. Phys.* **135**, 164705 (2011).
- [60] I. Fukuda, Zero-multipole summation method for efficiently estimating electrostatic interactions in molecular system, *J. Chem. Phys.* **139**, 174107 (2013).
- [61] P. Guo, R. Sknepnek, and M. Olvera de la Cruz, Electrostatic-driven ridge formation on nanoparticles coated with charged end-group ligands, *J. Phys. Chem. C* **115**, 6484 (2011).
- [62] T. K. Lytle, M. Radhakrishna, and C. E. Sing, High charge density coacervate assembly via hybrid Monte Carlo single chain in mean field theory, *Macromolecules* **49**, 9693 (2016).
- [63] A. Nikitin, Non-zero Lennard-Jones parameters for the Toukan-Rahman water model: More accurate calculations of the solvation free energy of organic substances, *J. Comput.-Aided Mol. Des.* **34**, 437 (2020).
- [64] N. Kamiya, I. Fukuda, and H. Nakamura, Application of zero-dipole summation method to molecular dynamics simulations of a membrane protein system, *Chem. Phys. Lett.* **568-569**, 26 (2013).
- [65] G. S. Demyanov and P. R. Levashov, Systematic derivation of angular-averaged Ewald potential, [arXiv:2203.15025v2](https://arxiv.org/abs/2203.15025v2) (2022).
- [66] E. Yakub and C. Ronchi, A new method for computation of long ranged Coulomb forces in computer simulation of disordered systems, *J. Low Temp. Phys.* **139**, 633 (2005).
- [67] J. D. Gale and A. L. Rohl, The general utility lattice program (GULP), *Mol. Simul.* **29**, 291 (2003).
- [68] R. J. Sadus, *Molecular Simulation of Fluids: Theory, Algorithms and Object-Oriented* (Elsevier Science, New York, 1999).
- [69] N. Metropolis, A. W. Rosenbluth, M. N. Rosenbluth, A. H. Teller, and E. Teller, Equation of state calculations by fast computing machines, *J. Chem. Phys.* **21**, 1087 (1953).
- [70] H. Gould and J. Tobochnik, *An Introduction to Computer Simulation Methods: Applications to Physical Systems*, 2nd ed. (Addison-Wesley, Reading, MA, 1996).